Detection of breast cancer based on novel porous silicon Bragg reflector surface-enhanced Raman spectroscopy-active structure

Xiaorong Ma (马小荣)[1], Hong Cheng (程 虹)[2], Junwei Hou (侯军伟)[3], Zhenhong Jia (贾振红)[4,*], Guohua Wu (吴国华)[5], Xiaoyi Lü (吕小毅)[4,], Hongyi Li (李弘毅)[6], Xiangxiang Zheng (郑向向)[5], and Chen Chen (陈 晨)[4]**

[1]*School of Physical Science and Technology, Xinjiang University, Urumqi 830046, China*
[2]*Affiliated Tumor Hospital of Xinjiang Medical University, Urumqi 830000, China*
[3]*Department of Engineering, China University of Petroleum-Beijing, Keramayi 834000, China*
[4]*School of Information Science and Engineering, Xinjiang University, Urumqi 830046, China*
[5]*School of Electronic Engineering, Beijing University of Posts and Telecommunications, Beijing 100876, China*
[6]*Quality of Products Supervision and Inspection Institute, Urumqi 830011, China*
**Corresponding author: jzhh@xju.edu.cn; **corresponding author: xiaoz813@163.com*
Received November 28, 2019; accepted January 16, 2020; posted online May 4, 2020

In this Letter, the surface-enhanced Raman scattering (SERS) signal of early breast cancer (BRC) patient serum is obtained by a composite silver nanoparticles (Ag NPs) PSi Bragg reflector SERS substrate. Based on these advantages, the serum SERS signals of 30 normal people and 30 early BRC patients were detected by this substrate. After a baseline correction of the experimental data, principal component analysis and linear discriminant analysis were used to complete the data processing. The results showed that the diagnostic accuracy, specificity, and sensitivity of the composite Ag NPs PSi Bragg reflector SERS substrate were 95%, 96.7%, and 93.3%, respectively. The results of this exploratory study prove that the detection of early BRC serum based on a composite Ag NPs PSi Bragg reflector SERS substrate is with a stable strong SERS signal, and an unmarked and noninvasive BRC diagnosis technology. In the future, this technology can serve as a noninvasive clinical tool to detect cancer diseases and have a considerable impact on clinical medical detection.

Keywords: porous silicon Bragg reflector; surface-enhanced Raman scattering; breast cancer detection; principal component analysis; linear discriminant analysis.
doi: 10.3788/COL202018.051701.

Breast cancer (BRC) is one of the most important malignant tumors affecting women's health. The number of BRC deaths worldwide is approximately 520,000 per year[1]. According to a report by the World Health Organization's International Agency for Research on Cancer in 184 countries and regions, the number of women with BRC in China is only smaller than that of the United States, which accounts for 11.9% of the world's total. Although people have an increasing knowledge of BRC and more diversified treatment methods in the past 20 years, the incidence and mortality still exhibit a substantial increase[2]. One of the reasons for this problem is that patients are diagnosed with BRC quite late[3], and the current diagnosis of BRC is determined by the patient's clinical manifestations and medical history, physical examination, imaging examination, X-ray, magnetic resonance imaging, or ultrasound, histopathology, and cytopathology[4]. However, these diagnostic techniques have insurmountable disadvantages. High cost and information lag have a great impact on the early diagnosis of BRC, causing patients to miss the best treatment time, and operative biopsy greatly deepens the patients' pain[5]. Therefore, it is of great significance to develop a low-cost technology that can diagnose BRC efficiently and reduce pain.

Many research groups have developed BRC serum diagnostic techniques based on surface-enhanced Raman scattering (SERS) and infrared spectroscopy. Raman spectroscopy is a detection method with a "fingerprint" recognition ability for the detection of each molecule or sample, which shows that the Raman spectroscopy detector itself has a better specificity[6]. For example, Shafer-Peltier *et al.* obtained human BRC tissue from *in vitro* samples and detected BRC tissue using SERS technology[7]. Many researchers, such as Vargas-Obieta, mixed the BRC serum with gold glue or silver glue and detected BRC serum using the SERS technique[8]. Zheng *et al.* used a microfluidic chip to detect BRC serum by SERS[9]. However, the sensitivity, stability, biocompatibility, and enhancement of the Raman peak in these detection methods are unsatisfactory.

The substrate is critical in the application of SERS, and researchers in various countries are still exploring new low-cost and high-enhancement substrates[10]. One type of porous substrates that have attracted much interest because of their impressive properties for sensor applications is a PSi-based device. The most attractive feature of PSi is its compatibility to be used with the biomolecules, and it is widely applied to biological and biomedical research[11].

The main reason for choosing a PSi nanomaterial is that PSi has rough surface characteristics. The PSi Bragg reflector can be prepared by controlling the corrosion current, which is simple to operate and has a low cost[12]. Yue *et al.* prepared a single-layer PSi substrate and used it to detect echinococcosis serum[13]. Zhang *et al.* developed a PSi optical microcavity biosensor for detecting DNA and the detection limit is 43.9 nmol/L[14]. Futamata *et al.* achieved SERS detection of rhodamine 6G (R6G) molecules on single-layer PSi substrates[15]. Wang *et al.* developed a PSi surface grating and applied it to SERS research[16]. For these advantages, PSi materials can be used as a good SERS substrate.

In this Letter, a composite silver nanoparticles (Ag NPs) PSi Bragg reflector SERS substrate is experimentally optimized. N-type highly doped silicon wafers[17] with a greater porosity and specific surface area cannot only be used for SERS detection of macromolecular organisms but can also greatly improve SERS signal intensity[18]. At the same time, the substrate offers a high detection sensitivity, which is of great significance for the diagnosis of BRC. Finally, and more importantly, this Letter uses the composite Ag NPs PSi Bragg reflector SERS substrate to detect the early BRC serum collected in the clinic and uses the principal component analysis (PCA) and linear discriminant analysis (LDA) (PCA-LDA) method to carry out statistical analysis and calculate results to show that the accuracy, specificity, and sensitivity of the diagnosis are 95%, 96.7%, and 93.3%, respectively. Analysis of the data better shows that the optimized SERS substrate has a high accuracy and practicability, and this detection technology can serve as a new noninvasive clinical tool for cancer detection and make a great contribution to clinical medicine.

All serum samples were acquired from the First Affiliated Hospital of Xinjiang Medical University. Approval of the ethics committee was obtained to study human blood serum samples. In our experiment, 30 samples of fresh blood from early BRC patient serum and 30 samples of fresh blood from normal subjects were obtained. 3 mL fresh blood was collected from each patient without any anticoagulant, and the samples were placed in a clean environment at 37°C for 1 h for condensing. Then, a high-speed centrifuge (4000 r/min) was used to centrifuge the blood at 4°C for 5 min, and the top level of clear liquid was extracted to obtain the serum. The serum was subpacked in a centrifuge tube and stored in a refrigerator at −80°C for experiments.

To better verify the sensitivity of the substrate, we diluted the early BRC serum with deionized water in terms of volume ratio and placed it on an oscillator for 20 min to mix it evenly. We took the early BRC serum out of the freezer and diluted it immediately after ablation to prevent inactivation, and pipette 2 μL of it onto the prepared substrates. (The preparation process of composite Ag NPs PSi Bragg reflector SERS substrate is shown in the Supplementary Materials.)

The serum Raman spectra were recorded using a confocal Raman microspectrometer (LabRAM HR Evolution Raman spectrometer, HORIBA Scientific, Ltd.) with an excitation wavelength of 532 nm and an Ar^+ laser (12.5 mW). The spectral data were acquired in 5 s with a 50× objective, and the numerical aperture (NA) was 0.5. Three spectra were recorded for each sample in different positions, and the mean spectrum was taken for further analysis.

Figure 1 shows the SEM images of the SERS substrates. Figure 1(a) indicates that the PSi substrate has a uniform pore distribution, and the pore size is 40–70 nm. Figure 1(b) shows that the thickness of the PSi film is approximately 3.8 μm. It can be observed from Fig. 1(c) that this substrate is more conducive to reaching deeper layers, thus providing high-performance detection for medical diseases. Figure 1(d) shows the surface morphology of $AgNO_3$ solution concentrations of 0.05 mol/L. The size of the Ag NPs is suitable for being well embedded into PSi, and the spacing between the Ag NPs is relatively uniform.

Figure 2 shows the SERS spectra of early BRC serum samples from 30 patients on the silicon substrates, the single-layer PSi SERS substrates, and the composite Ag NPs PSi Bragg reflector SERS substrate. The results show that the Raman scattering signal from the composite Ag NPs PSi Bragg reflector SERS substrate is obviously enhanced. For the Raman peak of 1157 cm^{-1}, the enhancement coefficient on the composite Ag NPs PSi Bragg reflector SERS substrate is 3.17 times higher than that on the single-layer PSi SERS substrate.

The composite Ag NPs PSi Bragg reflector SERS substrate can enhance the SERS effect of the analyte[19]. The periodic change of the refractive index of the PSi Bragg structure increases the interaction time between light and material, enhances the magnetization, and improves the SERS signal intensity[20]. Our research team carried out X-ray diffraction detection and theoretically simulated the electric field distribution on single-layer PSi and

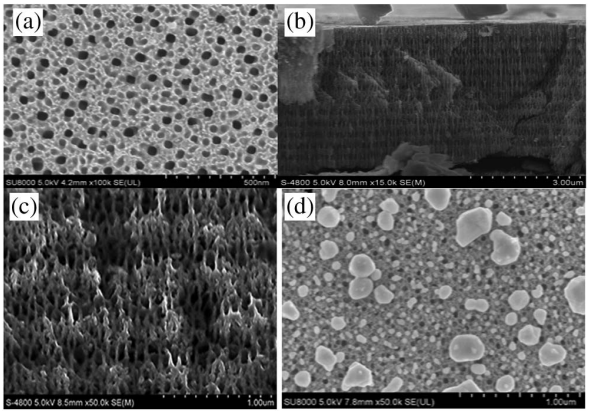

Fig. 1. SEM images of the newly prepared SERS substrates: (a) surface morphology; (b) cross-sectional morphology; (c) partial enlarged view of (b); (d) surface morphology of the composite Ag NPs PSi Bragg reflector SERS substrate.

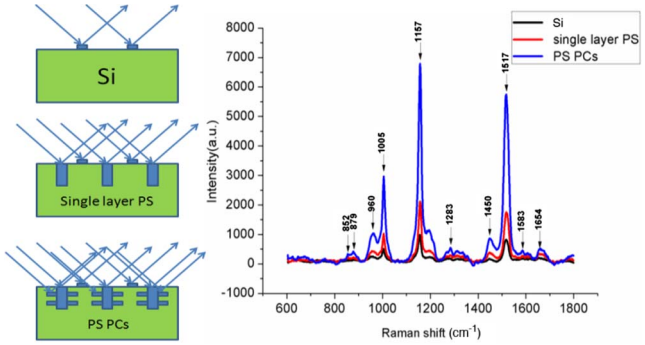

Fig. 2. SERS spectra of early BRC serum samples from 30 patients on monocrystalline silicon, composite Ag NPs single-layer PSi substrates, and the composite Ag NPs PSi Bragg reflector SERS substrate.

multi-layer PSi. Though the calculation simulation and detection results showed that the diffraction peaks of the multi-layer PSi became wider and wider, the field intensity of the PSi photonic crystals was stronger than that of single-layer PSi[17,21]. It was proved by experiments and calculation simulation that the enhanced electric field on the surface of photonic crystals is conducive to achieving a stronger localized surface plasmon resonance (LSPR), which leads to the enhancement of Raman optical signals.

Figure 3 shows the SERS spectra of early BRC serum samples (diluted in different proportions) on the composite Ag NPs PSi Bragg reflector SERS substrate. The SERS spectra of normal human serum samples (diluted in different proportions) were tested on the composite Ag NPs PSi Bragg reflector SERS substrate (see Fig. S2 in the Supplementary Materials). A Raman signal can be obtained on all samples. Therefore, the substrate has a high detection sensitivity. The vibration modes of the characteristic peaks in the early BRC serum Raman spectra are summarized (see Table S1 in the Supplementary Materials). It is found that the detection

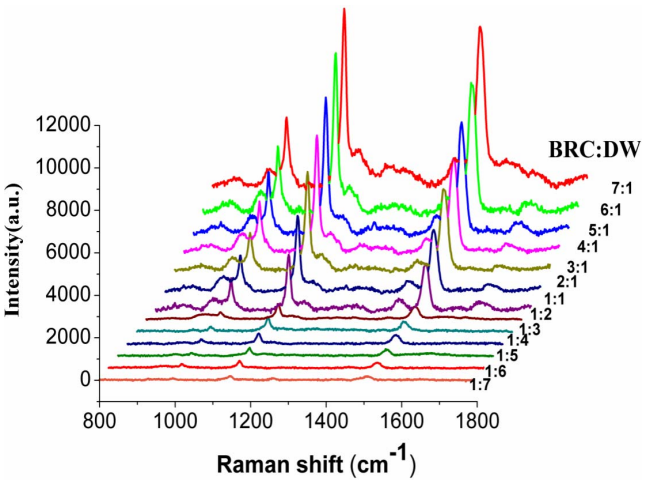

Fig. 3. SERS spectra of early BRC serum samples (diluted in different proportions) on the composite Ag NPs PSi Bragg reflector SERS substrate.

limit was reached when the concentration diluted to BRC: DW of 1:7. In addition, the substrate can also be used to detect different concentrations of R6G probe molecules and calculate the Raman enhancement factor (EF) of its SERS substrate (see Fig. S3 in the Supplementary Materials). The EF of 10^{11} SERS for R6G is calculated from the supplementary material.

The serum SERS spectra of 30 normal persons and 30 early BRC patients were analyzed by principal component analysis combined with linear discriminant analysis (PCA-LDA). And we have made the difference graph of the average normalized spectrum between the serum of healthy people and the early BRC patients (see Fig. S4 in the Supplementary Materials). It can be intuitively seen that the average normalized spectrum of serum of healthy people and early BRC patients has some differences in some Raman characteristic peaks. This provides a theoretical basis for further classification through algorithms.

First, the original spectral signal was corrected by LabSpec6 software and then normalized between 0 and 1 to reduce the influence of the laser power fluctuation and the slight differences in experimental conditions. Then, PCA was used to reduce the dimension of the $600-1800\,\mathrm{cm}^{-1}$ band of interest, and the characteristic spectrum that best reflected the difference between normal people and BRC patients was identified for subsequent discriminant analysis.

The first three principal components (PC1, PC2, and PC3) with the largest variance contribution rate after PCA were selected for analysis. In Figs. 4(a)–4(c), two dimensional scatter plots were made with PC1 and PC2, PC1 and PC3, and PC2 and PC3 as monocrystalline X and Y axes, respectively. Figure 4(d) shows a three-dimensional scatter plot based on the X, Y and Z axes

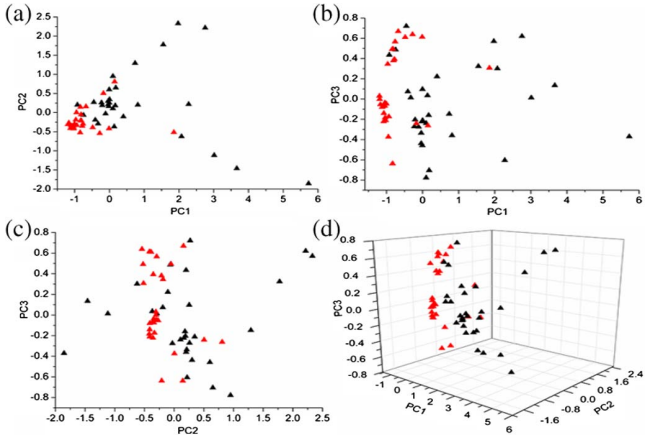

Fig. 4. (a) Plot of PC1 versus PC2 for the normal group versus the BRC group. (b) Plot of PC1 versus PC3 for the normal group versus the BRC group. (c) Plot of PC2 versus PC3 for the normal group versus the BRC group. (d) A three-dimensional mapping of the PCA results for the normal group and BRC group with PC1, PC2, and PC3 as the three axes. (The black triangle represents the normal group; the red triangle represents the BRC group.)

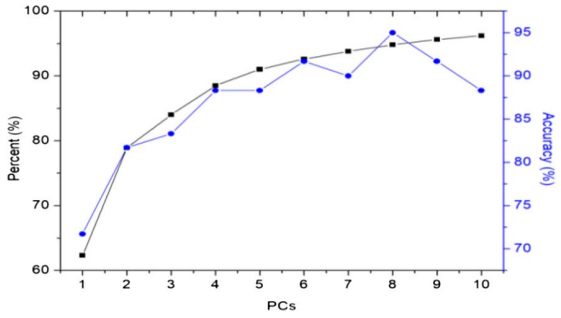

Fig. 5. Cumulative variance contribution rate and LDA classification accuracy as a function of the number of principal components.

of PC1, PC2, and PC3. After PCA treatment, there is a certain distinction between normal people and early BRC patients, which indicates the feasibility of using the serum SERS spectrum to screen early BRC patients based on the developed substrate here. However, it can also be seen that there is still some overlap between healthy people and early BRC patients. To achieve better diagnostic specificity and sensitivity, further analysis is needed by LDA.

Generally, the accuracy of discriminant analysis increases with the number of principal components after dimensionality reduction[22]. The number of principal components increases (from PC1 to PC10); the cumulative variance contribution rate and the accuracy of LDA are shown in Fig. 5. When the selected number of principal components is 8, the LDA achieves the best classification accuracy of 95% and the cumulative variance contribution rate is 94.8%. Therefore, the first eight principal components were selected for subsequent LDA.

Considering the small sample size, to obtain more reliable diagnostic results, LDA uses the leave one out cross validation (LOOCV) method[22]. Table 1 shows the first eight principal components using LOOCV LDA. Two out of 30 healthy persons were misdiagnosed with BRC (false positive), and only one out of 30 early BRC patients was misdiagnosed (false negative). Therefore, the diagnostic sensitivity, specificity, and total accuracy of PCA-LDA are 93.3%, 96.7%, and 95%, respectively.

In this Letter, the composite Ag NPs PSi Bragg reflector SERS substrate was successfully prepared by electrochemical etching and chemical reduction. The SERS response of the serum for 30 normal people and 30 early BRC patients was measured on the composite Ag NPs PSi Bragg reflector SERS substrate, and statistical analysis was carried out by PCA-LDA. The analysis results show that the diagnostic sensitivity is 93.3%, the specificity is 96.7%, and the total accuracy is 95%. The images show that the Raman signal intensity on the composite Ag NPs PSi Bragg reflector SERS substrate is more than three times higher than that on the single-layer PSi SERS substrate. The results of this exploratory study prove that the detection of early BRC serum based on a composite Ag NPs PSi Bragg reflector SERS substrate is with a stable, strong Raman signal, and an unmarked and noninvasive BRC diagnosis technology. In the future, this detection technology can serve as a noninvasive clinical tool for cancer detection, and its use can extend to food safety, jewelry identification, cultural relics identification, and other fields.

Table 1. Confusion Matrix for the LDA Algorithm[22]

		Histopathological reference class	
Confusion matrix		Normal	Cancer
Predicted class	Normal	28	2
	Cancer	1	29
Cross validation (%)	Normal	93.3	6.7
	Cancer	3.3	96.7

This work was supported by the National Natural Science Foundation of China (Nos. 61665012, 61575168, and 61765014), the International Science Cooperation Project of the Ministry of Education of the People's Republic of China (No. 2016–2196), and the Reserve Talents Project of National High-level Personnel of the Special Support Program (No. QN2016YX0324).

References

1. J. Ferlay, I. Soerjomataram, R. Dikshit, S. Eser, C. Mathers, M. Rebelo, D. M. Parkin, D. Forman, and F. Bray, Int. J. Cancer **136**, E359 (2015).
2. B. Freddie, R. Jian-Song, M. Eric, and F. Jacques, Int. J. Cancer **132**, 1133 (2013).
3. K. R. Bauer, M. Brown, R. D. Cress, C. A. Parise, and V. Caggiano, Cancer **109**, 1721 (2010).
4. M. F. Ernst and J. A. Roukema, Breast **11**, 13 (2002).
5. J. S. Drukteinis, B. P. Mooney, C. I. Flowers, and R. A. Gatenby, Am. J. Med. **126**, 472 (2013).
6. H. Cai, X. Yu, Q. Chu, Z. Jin, B. Lin, and G. Wang, Chin. Opt. Lett. **17**, 110601 (2019)
7. K. E. Shafer-Peltier, A. S. Haka, M. Fitzmaurice, J. Crowe, J. Myles, R. R. Dasari, and M. S. Feld, J. Raman Spectrosc. **33**, 552 (2002).
8. E. Vargas-Obieta, J. C. Martínez-Espinosa, B. E. Martínez-Zerega, L. F. Jave-Suárez, A. Aguilar-Lemarroy, and J. L. González-Solís, Lasers Med. Sci. **31**, 1317 (2016).
9. Z. Zheng, W. Lei, L. Lang, S. Zong, Z. Wang, and Y. Cui, Talanta **188**, 507 (2018).
10. Y. Lu, X. Kan, T. Xu, J. Fang, M. Wang, C. Yin, and X. Chen, Chin. Opt. Lett. **16**, 012301 (2018).
11. F. Peng, Y. Su, Y. Zhong, C. Fan, S.-T. Lee, and Y. He, Acc. Chem. Res. **47**, 612 (2013).
12. H. Lin, J. Mock, D. Smith, T. Gao, and M. J. Sailor, J. Phys. Chem. B **108**, 11654 (2004).
13. X. Yue, X. Zheng, G. Lv, J. Mo, X. Yu, J. Liu, Z. Jia, X. Lv, and J. Tang, Optik **192**, 162959 (2019).
14. H. Zhang, Z. Jia, X. Lv, J. Zhou, and J. Ma, Biosens. Bioelectron. **44C**, 89 (2013).
15. M. Futamata and Y. Maruyama, Appl. Phys. B **93**, 117 (2008).
16. J. Wang, Z. Jia, and C. Lv, Opt. Express **26**, 6507 (2018).

17. F. Zhong, Z. Wu, J. Guo, and D. Jia, Nanomaterials (Basel) **8**, 872 (2018).
18. A. Y. Panarin, S. N. Terekhov, K. I. Kholostov, and V. P. Bondarenko, Appl. Surface Sci. **256**, 6969 (2010).
19. S. Lin, W. Zhu, Y. Jin, and K. B. Crozier, Nano Lett. **13**, 559 (2013).
20. X. Fan, J. Jiang, X. Zhang, K. Liu, S. Wang, and T. Liu, Chin. Opt. Lett. **17**, 120603 (2019).
21. X. Yue, H. Li, X. Lv, and J. Tang, Opt. Mater. **2**, 100027 (2019).
22. X. Zheng, G. Lv, Y. Zhang, X. Lv, Z. Gao, J. Tang, and J. Mo, Spectrochim. Acta A **215**, 244 (2019).